

A morphoelastic model for dermal wound closure

L. G. Bowden¹ · H. M. Byrne¹ · P. K. Maini¹ · D. E. Moulton¹

Received: 22 May 2015 / Accepted: 1 August 2015 / Published online: 12 August 2015
© Springer-Verlag Berlin Heidelberg 2015

Abstract We develop a model of wound healing in the framework of finite elasticity, focussing our attention on the processes of growth and contraction in the dermal layer of the skin. The dermal tissue is treated as a hyperelastic cylinder that surrounds the wound and is subject to symmetric deformations. By considering the initial recoil that is observed upon the application of a circular wound, we estimate the degree of residual tension in the skin and build an evolution law for mechanosensitive growth of the dermal tissue. Contraction of the wound is governed by a phenomenological law in which radial pressure is prescribed at the wound edge. The model reproduces three main phases of the healing process. Initially, the wound recoils due to residual stress in the surrounding tissue; the wound then heals as a result of contraction and growth; and finally, healing slows as contraction and growth decrease. Over a longer time period, the surrounding tissue remodels, returning to the residually stressed state. We identify the steady state growth profile associated with this remodelled state. The model is then used to predict the outcome of rewounding experiments designed to quantify the amount of stress in the tissue, and also to simulate the application of pressure treatments.

Keywords Finite elasticity · Wound healing · Dermis · Volumetric growth · Contraction

1 Introduction

Wound healing is the physiological process by which damaged tissue repairs and regenerates. Most commonly, this tissue is the skin and the damage is caused by controlled surgical procedures or traumatic accident. In either case, it is desirable for the wound to heal quickly and efficiently, restoring the skin's mechanical, protective, and regulatory functions. The estimated cost of pathological wound-related surgical procedures and subsequent treatment is a staggering £1 billion a year in the UK alone (Hex et al. 2012).

Surface wounds break only the outermost layer of the skin, the epidermis. Epidermal wounds usually heal without complications by proliferation and migration of epithelial cells across the defect. More problematic are wounds that also damage the underlying dermis, a thicker layer of collagenous elastic tissue.

Wound contraction is responsible for up to 80 % of dermal healing (McGrath and Simon 1983). The main process by which this occurs is fibroblasts pulling the wound edges inwards. Additionally, growth of new tissue within the surrounding healthy dermis, also regulated by fibroblasts, may contribute to healing. The hole that remains is initially filled with extracellular matrix and over a longer period of time is remodelled into scar tissue.

Immediately after injury, the residual tension in the skin is released at the wound edge, causing retraction of the wound edge (McGrath and Simon 1983). Healing then proceeds through four main overlapping phases: haemostasis, inflammation, proliferation, and remodelling. Firstly, haemostasis is the formation of a blood clot in the wound space. This forms within hours of wounding, is made primarily of fibrin, and prevents blood loss. The clot acts as a source of blood-derived chemotactic factors which initiate the migration of inflammatory cells into the wound space

✉ L. G. Bowden
bowden@maths.ox.ac.uk

¹ Wolfson Centre for Mathematical Biology, Mathematical Institute, University of Oxford, Andrew Wiles Building, Radcliffe Observatory Quarter, Woodstock Road, Oxford OX2 6GG, UK

(Wahl et al. 1989). The inflammatory phase lasts for up to a week (Jeffcoate et al. 2004) during which inflammatory cells clear the wound site of bacteria, dead tissue, and other foreign bodies (Singer and Clark 1999). Fibroblasts naturally present in the surrounding dermal tissue proliferate in response to growth factors secreted by inflammatory cells (Clark 1988) and migrate up the chemotactic gradient created by chemoattractants from the fibrin clot. Fibroblasts initiate the formation of collagen fibres that increase the mass of the dermal tissue. Epithelial cells migrate and proliferate into the wound in response to growth factors. This process, termed re-epithelialisation, ensures that an epidermal covering is restored. Contraction of the wound edge begins approximately 2–5 days post-wounding (Monaco and Lawrence 2003) as fibroblasts arranged at the wound edge crawl across the substratum towards the wound centre resulting in an inward movement of the dermal edges. Many of the fibroblasts infiltrate and break down the fibrin clot, replacing it with a collagen-rich matrix or scar tissue. Even after the wound has healed, the scar and surrounding tissue remodel over several months. This process is important aesthetically and further allows the tissue to regain mechanical integrity.

Wound healing has been studied in a mathematical and computational context for over 20 years. Developing accurate mathematical models of wound healing that can be validated experimentally can play a crucial role in understanding and exploring the mechanisms driving healing. Sherratt and Murray (1990) were the first to translate this biological phenomenon into mathematical terms, formulating reaction-diffusion equations to describe epidermal wound healing. Extensions to this model saw an investigation into healing rates and patterns for various wound shapes (Sherratt and Murray 1992). For full thickness wounds, mathematical models typically focus on one of the processes contributing to dermal healing, for example wound contraction (Tranquillo and Murray 1992; Tracqui et al. 1995; Olsen et al. 1999; Yang et al. 2013) or tissue synthesis (Segal et al. 2012). There are two main approaches to modelling wound contraction. One is through partial differential equation models (PDEs) based on the principles of mass and momentum balance. Typically, these couple mass balances for the density of fibroblasts and extracellular matrix (ECM) with a momentum balance for the displacement of the cell–ECM continuum and constitutive laws that define the mechanical properties of the tissue (Tranquillo and Murray 1992; Olsen et al. 1999). The second approach is based on a hybrid framework. Models of this kind focus on the interactions between fibroblasts, considered as discrete entities, and the ECM, considered as a continuous variable. The direction of fibroblast migration is governed by ECM fibre orientation, which cells can change (Dallon et al. 1999; Dallon 2000; McDougall et al. 2006). Although most models of wound healing are formulated either as sys-

tems of PDEs or as hybrid models, other less widely used approaches merit discussion. For example, Segal et al. (2012) studied the contribution of collagen accumulation in a wound to healing of the tissue. Their spatially averaged model consisted of a system of time-dependent, ordinary differential equations (ODEs). Although the complexity was reduced by adopting a spatially averaged framework, the model still had a large number of parameters that needed to be determined experimentally.

The various processes contributing to healing overlap; therefore, models that combine these processes may offer a more in-depth understanding of wound healing. Vermolen and Javierre (2012) adapted and coupled previous models of wound contraction (Tranquillo and Murray 1992), angiogenesis (Maggelakis 2004), and epidermal wound closure (Sherratt and Murray 1991) to provide a descriptive model of dermal regeneration. The authors used their model to investigate the effects of the various contributing processes to healing of the dermis. Although the model was more complete in that many processes were included, this came at the cost of an increased number of undetermined model parameters. We have previously adopted an ODE framework, focussing on the dominant processes contributing to healing of a full thickness wound (Bowden et al. 2014). A system of three ODEs was derived to track changes in the epidermal and dermal wound areas over time, coupled to a phenomenological force balance. Growth of new tissue was governed by a modified logistic growth law with dermal growth enhanced by mechanical stretch caused by contraction of the tissue. Although the model combined the effects of growth and contraction, and contained few parameters, it neglected spatial effects, which could play an important role in mechanosensitive growth.

In the models discussed above, mechanical effects are typically included via linear elasticity, if at all. Several factors highlight the importance of the mechanical environment in healing and the value of a nonlinear elastic modelling framework. When a circular wound is formed in mice, following injury the skin retracts causing the wound to increase to 120% of its initial area (McGrath and Simon 1983). The retraction implies the presence of residual tension in the skin that is released when the skin is cut, while the large degree of retraction points to a nonlinear regime. It is also known that growth can be stimulated by local changes in mechanical stress. Such stress is generated in healing tissue by wound contraction, largely driven by fibroblast activity at the wound edge. While models of wound contraction typically focus on the interior of the wound, e.g. the formation and remodelling of the central granulation tissue into scar tissue (Cumming et al. 2010; Yang et al. 2013), the “pulling” of the fibroblasts on the surrounding dermal tissue directly impacts the stress and growth in the tissue, which is crucial for the final size of the defect and the potential for scarring.

Morphoelasticity provides a theoretical framework for modelling growth in elastic tissues. It enables for a mathematically tractable approach for studying the growth and remodelling of elastic tissue, while allowing for large deformations, anisotropy, and heterogeneity. It has been applied to various biological tissues including arteries (Taber and Eggers 1996; Rachev et al. 1998; Taber 1998, 2001; Goriely and Vandiver 2010), the heart (Lin and Taber 1995), the trachea (Moulton and Goriely 2011), plant stems (Goriely et al. 2010), tumours (Ambrosi and Mollica 2004; Ciarletta et al. 2011), and the skin (Ciarletta and Ben Amar 2012). Despite this wide range of applications, few mathematical models of wound healing incorporate nonlinear elasticity. Yang et al. (2013) developed a biomechanical model of wound healing that focussed on the formation and remodelling of the scar tissue, which has nonlinear elastic properties. Wu and Ben Amar (2015) used the decomposition of the deformation tensor to study the closure of a circular epidermal wound and investigated stress-induced instabilities of the regular wound geometry. Contraction of the nonlinear elastic tissue was assumed to be generated by circumferential resorption analogous to a model of embryonic wound healing (Taber 2009) in which the author formulates mechanosensitive growth laws with an evolving target stress. The main focus of this paper is the development of a morphoelastic model of dermal closure, that accounts for growth and contraction. Although wounding also affects the epidermal layer, we do not explicitly model re-epithelialisation, incorporating only the effects of the epidermis on the dermis. By postulating mechanosensitive growth laws, we aim to understand how the mechanical environment in the dermal tissue surrounding the wound impacts the healing process. We use the model to gain mechanistic insights, investigate the feedback between growth and contraction in dermal closure, and predict behaviours that can be tested experimentally.

The paper is organised as follows. In Sect. 2, we develop the governing equations for the growth and mechanical equilibrium of the tissue, using the framework of morphoelasticity. The presence of volumetric growth is demonstrated by considerations of residual tension in the skin, and the form of mechanosensitive growth laws is motivated by a simple analysis of homogeneous growth. In Sect. 3, we present typical results of wound healing simulations. We show that the model can exhibit normal healing behaviour and show the effect of key parameters on healing. We also consider the possibility of tissue remodelling to a steady state of residual stress over a long timescale. We then use the model to predict the outcome of hypothetical rewounding experiments as a method of determining the stress in the tissue and the outcome of applying pressure to control wound closure. Conclusions and discussion are provided in Sect. 4.

2 Model description

In this section, we develop a mechanical model of dermal tissue subjected to a circular wound. We treat the dermal tissue as a cylindrical elastic annulus surrounding the wound such that the outer radius is far from the wound edge and the effects of dermal tissue external to the cylinder can be approximated by imposing a boundary condition at the outer edge. Our model is developed by considering the wound geometry, the tissue mechanics (balance of linear and angular momentum) and by prescribing constitutive laws relating stress to strain, and for growth.

2.1 Geometry

The geometry is pictured schematically in Fig. 1. In order to incorporate the presence of residual tension in the skin, we identify four states. The pre-wounded tissue is denoted by state S_1 —this tissue is in a state of residual tension, which for a finite cylinder can be assumed to arise from a pressure T_{res} applied by the external skin. If excised, the residual tension is relieved and the tissue relaxes to a stress-free configuration, denoted S_0 . We assume a wound of radius A is formed in the tissue at time $t = 0$, at which point the stress on the inner surface is relieved and the wound fully recoils to a radius a_R by time t_R —we refer to this configuration as state S_2 . Fibroblast activity then creates a contraction force f_c at the inner edge, so that at times $t > t_R$ the wound radius is a ; this current state is referred to as S_3 . Growth does not occur until contraction begins; thus, there is assumed to be no growth in states S_0, S_1, S_2 .

We restrict attention to symmetric deformations; thus, all configurations are described as cylindrical annuli. In particular, the radial and axial coordinates, R_0 and Z_0 , in the stress-free reference state (S_0) are deformed, at time t , to r and z in the current state (S_3). The geometrical region associated with the reference state is

$$A_0 \leq R_0 \leq B_0, \quad 0 \leq \Theta \leq 2\pi, \quad 0 \leq Z_0 \leq L_0,$$

where A_0 , B_0 , and L_0 denote the wound radius, the outer radius of the modelling domain, and the initial thickness of the tissue in the stress-free state, respectively. This region is deformed in the current state to

$$a \leq r \leq b, \quad 0 \leq \theta \leq 2\pi, \quad 0 \leq z \leq l,$$

by the maps

$$r = r(R_0, t), \quad \theta = \Theta, \quad z = \lambda(t)Z_0, \quad (1)$$

where λ is the axial stretch.

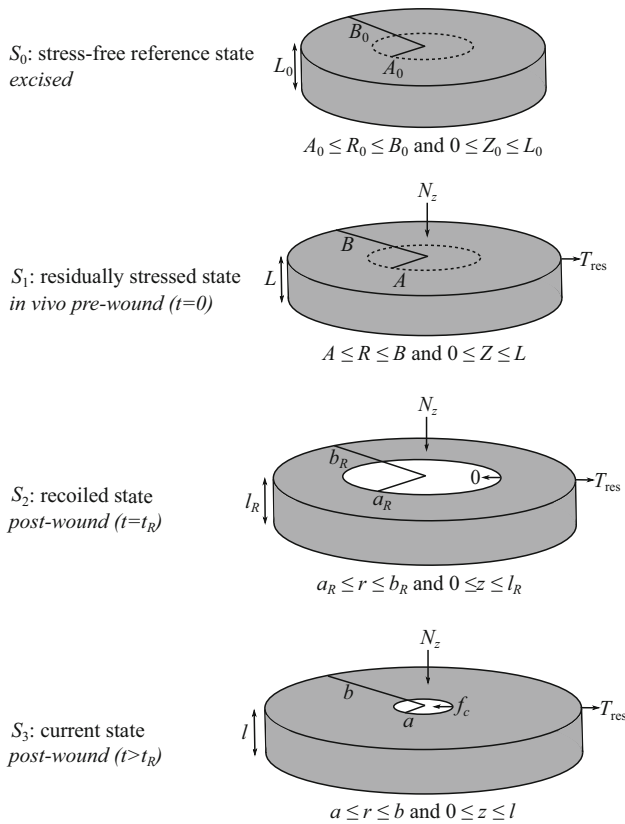


Fig. 1 Schematic representation of the mathematical model. Distance from the wound centre in the stress-free state can be described by the independent variable R_0 , where $A_0 \leq R_0 \leq B_0$. The cylinder represents the dermal tissue in which, under some deformation F , the reference state is mapped to the current state. Distance from the wound centre in the current state can be described by the dependent variable $r = r(R_0, t)$, where $a \leq r \leq b$, at time t . In vivo, the tissue is residually stressed with external radial pressure T_{res} MPa and axial load N_z N. After wounding, tension is released on the wound edge causing the wound to recoil, resulting in the recoiled state, where $a_R \leq r \leq b_R$. As the wound heals, it is subject to contraction modelled as a radial pressure, f_c MPa, on the wound edge. Far from the wound, the tissue remains residually stressed

2.2 Morphoelastic framework

Consider an elastic body which, in its reference state, is described by the material coordinates \mathbf{X} . After some deformation, the body in the current state is described by $\mathbf{x} = \mathbf{x}(\mathbf{X}, t)$. The map from the reference to the current state is described by the geometric deformation tensor (Rivlin 1948), $F = \frac{\partial \mathbf{x}}{\partial \mathbf{X}}$, which in a cylindrical geometry is given by

$$F = \text{diag} \left(\frac{\partial r}{\partial R_0}, \frac{r}{R_0}, \lambda \right). \tag{2}$$

Following the fundamental assumption of morphoelasticity, the deformation F is viewed as a combination of two processes (Rodriguez et al. 1994). The local addition (or

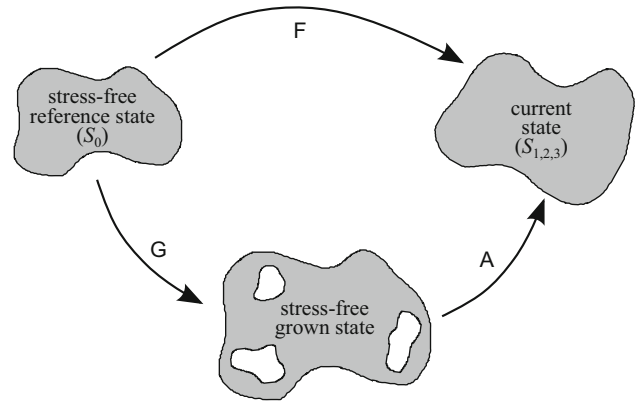


Fig. 2 A schematic representation of the deformation of an elastic body. The deformation tensor F can be decomposed into a growth tensor G , describing the local addition of material, and an elastic tensor A , describing the elastic response of the body. The deformation is applied to a stress-free state, corresponding to S_0 in Fig. 1, resulting in the current state. Depending on the deformation, the current state corresponds to S_1, S_2 , or S_3 in Fig. 1

removal) of material to the stress-free state, described by the growth tensor G , changes the mass of the body. To accommodate any growth incompatibilities that the body may undergo, we introduce an elastic deformation, described by the elastic tensor A . Thus, the geometric deformation tensor can be decomposed as $F = A \cdot G$, represented schematically in Fig. 2.

For symmetric deformations, we write the growth tensor as $G = \text{diag}(\gamma_r, \gamma_\theta, \gamma_z)$, where γ_r, γ_θ , and γ_z , represent radial, circumferential, and axial growth (or resorption), respectively. Note that each γ_i can be a function of position, such that $\gamma_i > 1$ (< 1) signifies a local increase (decrease) in mass in the direction i . The elastic tensor is given by $A = \text{diag}(\alpha_r, \alpha_\theta, \alpha_z)$, where α_r, α_θ , and α_z are the principle stretches in the radial, circumferential, and axial directions, respectively.

Mechanical testing has shown that the skin is almost incompressible (North and Gibson 1978), and so we assume $\det(A) = 1$. The deformation then satisfies

$$\frac{\partial r}{\partial R_0} = \frac{\gamma_r \gamma_\theta \gamma_z R_0}{\lambda r} \tag{3}$$

from which we ascertain

$$r^2(R_0) = a^2 + 2 \int_{A_0}^{R_0} \frac{\gamma_r(\tilde{R}) \gamma_\theta(\tilde{R}) \gamma_z(\tilde{R}) \tilde{R}}{\lambda} d\tilde{R}. \tag{4}$$

For given growth functions $\gamma_i(R_0)$, the deformation is fully determined once a and λ are known. The corresponding principle stretches of the elastic deformation tensor can be written as

$$\mathbf{A} = \text{diag} \left(\frac{\gamma_z}{\alpha\lambda}, \alpha, \frac{\lambda}{\gamma_z} \right), \quad \text{where } \alpha = \frac{r}{\gamma_\theta R_0}. \tag{5}$$

The system mechanics are described by the balance of linear and angular momentum and a constitutive stress–strain relationship. If the tissue has density ρ and is subject to body forces \mathbf{f}_b , the balance of linear momentum reads

$$\rho \ddot{\mathbf{x}} - \nabla \cdot \mathbf{T} - \rho \mathbf{f}_b = \mathbf{0}, \tag{6}$$

where a dot represents a derivative with respect to time. In Eq. (6), \mathbf{T} is the Cauchy stress tensor. The balance of angular momentum gives that \mathbf{T} is symmetric; in the cylindrical geometry, it is diagonal with radial, circumferential, and axial components denoted as T_{rr} , $T_{\theta\theta}$, and T_{zz} , respectively.

The stress–strain constitutive relationship for an incompressible hyperelastic material (Eringen 1962) is given by

$$\mathbf{T} = \mathbf{A} \cdot \frac{\partial W}{\partial \mathbf{A}} - p \mathbb{I}, \tag{7}$$

where the hydrostatic pressure p ensures incompressibility and $W = W(\alpha_r, \alpha_\theta, \alpha_z)$ is the strain-energy function. We model the dermal tissue as a neo-Hookean material (Rivlin 1948) with strain-energy function

$$W(\alpha_r, \alpha_\theta, \alpha_z) = \frac{\mu}{2} \left(\alpha_r^2 + \alpha_\theta^2 + \alpha_z^2 - 3 \right). \tag{8}$$

Expressing Eq. (7) in component form, we have

$$T_{rr} = \alpha_r W_r - p, \quad T_{\theta\theta} = \alpha_\theta W_\theta - p, \quad T_{zz} = \alpha_z W_z - p, \tag{9}$$

where $W_i = \partial W / \partial \alpha_i$.

The mechanical description is completed by prescribing appropriate boundary conditions. For example, we may specify the radial stress $T_{rr}|_{r=a,b}$ and/or the axial load, $N_z = \int T_{zz} \, dA$, with integration over the top of the annulus.

2.3 Residual stress

Implicit in the constitutive law in Eq. (7) is the assumption that \mathbf{F} describes a deformation from a stress-free reference state. Since the skin is naturally residually stressed in vivo, we require a map from the observed residually stressed state to the unknown stress-free state. In other words, S_1 is the typical observed pre-wound state, but the mechanical description entails a map from S_0 to S_3 ; hence, we must first determine the state S_0 . In this section, we determine the state S_0 and estimate the value of T_{res} by considering the initial recoil upon wounding. Typical wound healing data are given as a time series of averaged wound areas (Bowden et al. 2014) where initial measured quantities include the initial wound radius A , the recoiled wound radius a_R , and the tissue thickness L .

Given these measurements, the reference geometry and the residual stress can be calculated in the following way.

Let \mathbf{F}_1 and \mathbf{F}_2 denote the deformations from the stress-free state S_0 to the residually stressed (S_1) and recoiled (S_2) states, respectively, i.e. $\mathbf{F}_1 = \frac{\partial \mathbf{x}}{\partial \mathbf{X}_0}$ and $\mathbf{F}_2 = \frac{\partial \mathbf{x}_R}{\partial \mathbf{X}_0}$.

Assuming no body forces and that mechanical equilibrium is reached after the deformations \mathbf{F}_1 and \mathbf{F}_2 , Eq. (6) reads

$$\nabla \cdot \mathbf{T} = \mathbf{0}, \tag{10}$$

For plane stress, the only non-trivial component is

$$\frac{\partial T_{rr}}{\partial r} + \frac{1}{r} (T_{rr} - T_{\theta\theta}) = 0. \tag{11}$$

In state S_1 , the residual tension is assumed to be due to pressure at the external boundary, so that $T_{rr}(B_0) = T_{\text{res}}$.¹ Upon injury, the wound edge is relieved of tension, causing it to retract to a size bigger than that of the initial wound. Therefore, in the recoiled state S_2 , we have $T_{rr}(A_0) = 0$. Far from the wound, we expect the healthy dermis to remain residually stressed so that $T_{rr}(B_0) = T_{\text{res}}$ in S_2 .

The deformation \mathbf{F}_1 is found by solving Eq. (3) with $\mathbf{G} = \mathbb{I}$ (no growth has occurred yet)

$$R = \frac{R_0}{\sqrt{\lambda_1}}, \tag{12}$$

where λ_1 is the axial stretch associated with the deformation \mathbf{F}_1 and is determined by imposing $R(B_0) = B$ in Eq. (12), resulting in

$$R = \frac{B}{B_0} R_0. \tag{13}$$

The components of the elastic tensor are

$$\alpha_r = \alpha_\theta = \frac{B}{B_0}, \quad \text{and} \quad \alpha_z = \frac{B_0^2}{B^2}. \tag{14}$$

Since $\alpha_r = \alpha_\theta$, Eqs. (9) give $T_{rr} = T_{\theta\theta}$ and imposing $T_{rr}(B_0) = T_{\text{res}}$ in Eq. (11), we deduce that $T_{rr} \equiv T_{\text{res}}$ is constant. From Eq. (9), the axial stress is also constant and can be determined from the boundary condition

$$N_z = 2\pi \int_0^B T_{zz} R \, dR = \pi T_{zz} B^2. \tag{15}$$

If we assume no axial load in state S_1 ($N_z = 0$), then $T_{zz} = 0$ and the residually stressed state is one of constant planar isotropic stress with $\mathbf{T}^* = \text{diag}(T_{\text{res}}, T_{\text{res}}, 0)$.

¹ We note that there is a one-to-one map between all states. Our convention is generally to view all spatially dependent variables as functions of the independent variable R_0 . So, for example, we write $T_{rr}(R)$ as $T_{rr}(R_0) = T_{rr}(R(R_0))$.

For a neo-Hookean material with $N_z = 0$, Eqs. (8), (9), and (14) imply

$$T_{res} + \mu \left(\frac{B_0^4}{B^4} - \frac{B^2}{B_0^2} \right) = 0. \tag{16}$$

For the deformation F_2 , Eq. (4) with $\mathbf{G} = \mathbb{I}$ and $r(A_0) = a_R$ gives

$$r^2 = \frac{R_0^2 - A_0^2}{\lambda_2} + a_R^2, \tag{17}$$

where λ_2 is the axial stretch associated with the deformation F_2 . The radial stress is determined by substituting Eqs. (8) and (9) into Eq. (11) and integrating subject to $T_{rr}|_{r=a_R} = 0$:

$$T_{rr} = \frac{\mu}{2\lambda_2} \left[\log \left(\frac{\lambda_2(r^2 - a_R^2) + A_0^2}{A_0^2} \right) - \log \left(\frac{r^2}{a_R^2} \right) + \left(\frac{A_0^2}{\lambda_2} - a_R^2 \right) \left(\frac{1}{r^2} - \frac{1}{a_R^2} \right) \right] \tag{18}$$

We also have the axial boundary condition

$$N_z = 2\pi \int_a^b T_{zz} r \, dr = 0 \tag{19}$$

with $T_{zz} = T_{rr} + \alpha_z W_z - \alpha_r W_r$ from Eq. (9). Imposing $T_{rr}|_{r=b_R} = T_{res}$, Eqs. (16) and (18) can then be equated to eliminate T_{res} , giving

$$\frac{1}{2\lambda_2} \left[\log \left(\frac{B^2}{A^2} \right) - \log \left(\frac{b_R^2}{a_R^2} \right) + \left(\frac{A_0^2}{\lambda_2} - a_R^2 \right) \left(\frac{1}{b_R^2} - \frac{1}{a_R^2} \right) \right] + \left(\frac{B_0^4}{B^4} - \frac{B^2}{B_0^2} \right) = 0. \tag{20}$$

Given the measurements of the initial and recoiled wound radii, A and a_R , the thickness of the tissue, L , in vivo, the tissue stiffness, μ , and the outer radius, B , Eqs. (16), (19), and (20) can be solved simultaneously for T_{res} , B_0 , and λ . The stress-free reference geometry, $\{A_0, B_0, L_0\}$, and the residual stress, T_{res} , are then fully determined.

2.4 Domain size

From Eq. (16), we note that the residual stress depends on the outer radius B . However, we expect this to saturate with large B ; thus, we seek a domain size large enough that T_{res} in Eq. (16) is not affected by small changes in the location of the outer radius. Before continuing, we note that there exists a wide range of parameter values and wound sizes in the literature. This is partly due to measurements being taken from different species. Since most data available are

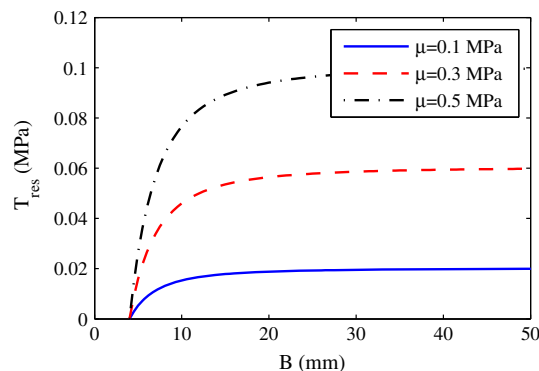


Fig. 3 Residual stress as a function of the outer radius. The residual stress is calculated according to Eq. (16) for a wound with $A = 4$ mm, $a_R = 4.4$ mm, and $L = 0.1$ mm for increasing B . The shear stress is $\mu = 0.1$ (solid line), $\mu = 0.3$ (dashed line), and $\mu = 0.5$ MPa (dotted dashed line). The calculated residual stress increases with shear stress and for large enough modelling domain T_{res} plateaus

for wound healing in mice, we choose our reference variables and parameter values accordingly. Following the experiments of McGrath and Simon (1983) (in which circular wounds in mice retract to a radius approximately 110 % of the initial cut), we take an initial wound radius $A = 4$ mm that recoils to $a_R = 4.4$ mm. For these values, we compute T_{res} in Eq. (16) while varying B —the result is plotted in Fig. 3 for three different choices of μ . We observe that T_{res} asymptotes as B increases; and thus assign the outer radius of the domain to $B = 20$ mm.

2.5 Shear elastic modulus

Measured values for the shear elastic modulus μ for dermal tissue may vary by a factor of 3000 depending on the model and experimental apparatus used (Diridollou et al. 2000). A large range of residual stress in the skin has also been reported, between 0.005 and 0.1 MPa (Diridollou et al. 2000; Jacquet et al. 2008; Flynn et al. 2011). As the stress has linear dependence on μ , we can use the residual stress calculation to estimate a physiological range for μ .

In Fig. 4, we plot T_{res} against μ . For $0.02 < \mu < 0.52$ MPa, the residual stress lies within the previously reported range $0.005 < T_{res} < 0.1$. Although the biological literature estimates that the shear stress can take values between 0.006 and 20 MPa, our model suggests that $\mu > 0.52$ MPa yields unphysiological values of the residual stress.

2.6 Contraction alone

The calculations of Sect. 2.3 have established the stress-free state and the residual tension. We can now turn to the healing of a wound. Our primary modelling aim is to explore mechanosensitive growth in the healing dermal tissue. This

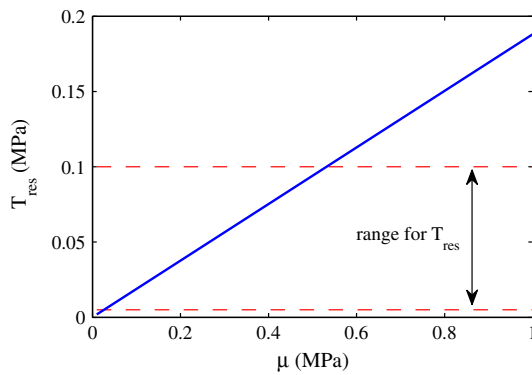


Fig. 4 Residual stress as a function of the shear elastic modulus. The residual stress is calculated according to Eq. (16) for a wound with $A = 4$ mm, $a_R = 4.4$ mm, and $L = 0.1$ mm for varying μ . For biologically realistic values of the residual stress as stated in the literature, the shear elastic modulus must lie in the range $0.02 < \mu < 0.52$ MPa

requires the definition of an evolution law for the growth tensor \mathbf{G} . To motivate this, as a starting point we consider the possibility that no growth occurs. That is, we suppose that wound closure is driven by contraction only, and we use the mechanical framework to quantify the degree of stress that would be generated in the tissue in this scenario.

Wound contraction in adult dermal wounds is driven by fibroblasts that localise on the wound edge and pull the tissue inwards (Ehrlich 1988; Ehrlich and Rajaratnam 1990). Dermal closure can reduce a wound by up to 80% of its original area. If there is no growth, we can simply impose a deformation from the post-wound state S_2 to an equilibrium configuration in which the wound radius has decreased by the appropriate amount. From Eqs. (8), (9), and (11), we deduce that the radial stress at the inner boundary required to deform the wound radius from its original size to its final contracted size a_c is given by

$$T_{rr}(A_0) = T_{res} - \frac{\mu}{2\lambda} \left[\log\left(\frac{B_0^2}{A_0^2}\right) - \log\left(\frac{B_0^2 - A_0^2 + \lambda a_c^2}{\lambda a_c^2}\right) \right] + (A_0^2 - \lambda a_c^2) \left(\frac{1}{B_0^2 - A_0^2 + \lambda a_c^2} - \frac{1}{\lambda a_c^2} \right), \quad (21)$$

where λ is determined by solving Eq. (19) and the reference variables A_0 and B_0 are as calculated in Sect. 2.3.

Mechanical testing reveals that, on average, mouse skin fails to withstand stresses higher than 2 MPa (Bermudez et al. 2011) and samples of dermis from diabetic mice tear at stresses as low as 0.5 MPa. In Fig. 5, we plot the stress at the inner edge as a function of μ . We find that, for a wide range of μ , the radial stress on the wound edge is higher than 0.5 MPa. This suggests that if healing occurs by contraction alone, then stresses higher than the tissue can withstand will be generated. Thus, for dermal closure to reduce a wound

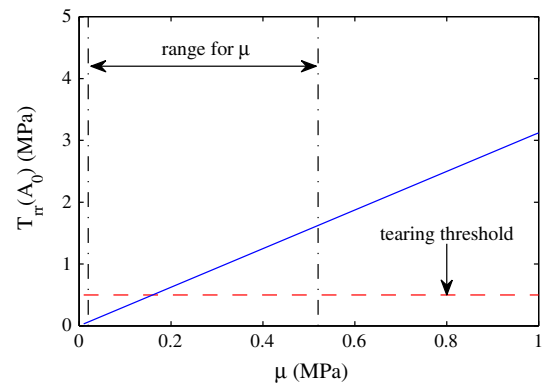


Fig. 5 Radial stress on the inner boundary required for dermal closure with no growth. Equation (21) is solved for varied values of μ and N_z with reference variables: $A = 4$ mm, $a_R = 4.4$ mm, $B = 20$ mm, and final wound radius $a_c = 1.8$ mm. For a wide range of parameter values, the radial stress calculated is higher than that the dermal tissue can physically withstand

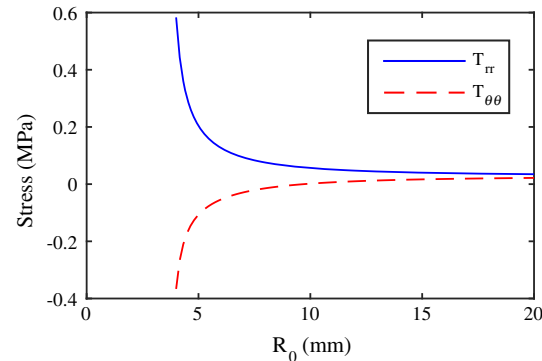


Fig. 6 Radial and circumferential stress for dermal closure with no growth. Equations (8), (9), and (11) are solved with $T_{rr}(B) = T_{res}$. We take $\mu = 0.2$ and $\lambda = 1$ with reference variables: $A = 4$ mm, $a_R = 4.4$ mm, $B = 20$ mm, and final wound radius $a_c = 1.8$ mm. The radial, T_{rr} , and circumferential, $T_{\theta\theta}$, stresses are plotted as functions of position

by up to 80%, volumetric growth must contribute to closure, relieving the high tension generated by contraction.

We further note that the circumferential stress at the wound edge can be computed from Eqs. (8), (9), and (21), revealing that it is highly compressive. This can be observed for the planar case ($\lambda = 1$) in Fig. 6 where we plot the radial and circumferential stresses as functions of position for contraction only.

2.7 Anisotropic homogeneous growth

Before proposing an evolution law for spatially dependent growth, it is instructive to analyse the effect of pure growth in a simple setting. We neglect all body forces and boundary loads and consider the effect of time-independent anisotropic but homogeneous planar growth on an annulus of tissue. That is, we take γ_r and γ_θ as constants (with $\gamma_z = 1$ and $\lambda = 1$)

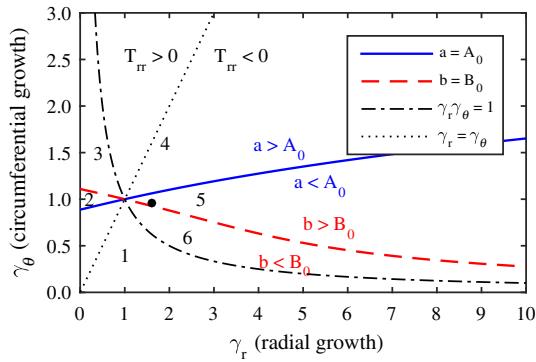


Fig. 7 Analysis of compatible growth laws. Equation (23) is solved numerically using the root-finding algorithm `fsolve` in `MATLAB` to find the curves in $(\gamma_r, \gamma_\theta)$ space such that $a = A_0$ (solid blue) and $b = B_0$ (dashed red). The dashed black line represents no growth, i.e. $\gamma_r \gamma_\theta = 1$. Regions 1 to 6 represent different grown configurations of the dermal cylinder. Reference variables are $A_0 = 4$ mm and $B_0 = 5$ mm corresponding to a proliferative band of width 1 mm surrounding the wound

and consider the deformation and stress state due to growth alone in the $(\gamma_r, \gamma_\theta)$ plane.

The deformation and stress satisfy

$$\frac{\partial r}{\partial R_0} = \gamma_r \gamma_\theta \frac{R_0}{r}, \tag{22a}$$

$$\frac{\partial T_{rr}}{\partial R_0} = \frac{\mu \gamma_r \gamma_\theta R_0}{r^2} \left(\frac{r^2}{\gamma_\theta^2 R_0^2} - \frac{\gamma_\theta^2 R_0^2}{r^2} \right), \tag{22b}$$

Solving Eqs. (22) subject to stress-free boundary conditions, we obtain an implicit equation for the current wound radius a in terms of γ_r, γ_θ , and the reference variables:

$$0 = \frac{\gamma_r}{2\gamma_\theta} \log\left(\frac{B_0^2}{A_0^2}\right) - \frac{\gamma_\theta}{2\gamma_r} \log\left(\frac{\gamma_r \gamma_\theta (B_0^2 - A_0^2) + a^2}{a^2}\right) + \frac{\gamma_\theta}{2\gamma_r} \left(a^2 - \gamma_r \gamma_\theta A_0^2 \right) \left(\frac{1}{a^2} - \frac{1}{\gamma_r \gamma_\theta (B_0^2 - A_0^2) + a^2} \right). \tag{23}$$

Similarly, we can obtain an implicit equation for the outer radius of the cylinder, b , by using Eq. (22a) to substitute for a . Equation (23) allows us to explore the effect of differential radial (γ_r) and circumferential (γ_θ) growth. In Fig. 7, we show how the $(\gamma_r, \gamma_\theta)$ parameter space can be decomposed into distinct regions, each associated with a different grown configuration.

For normal healing, the inner radius should decrease as the wound repairs. At the same time, the outer radius should not change markedly so that material is not compressed or pulled far from the wound. This behaviour with $a < A_0$ and $b \approx B_0$ corresponds to those parts of regions 5 or 6 in Fig. 7 that are close to the curve $b = B_0$. We observe that, close to the curve $b = B_0$, as γ_r increases, γ_θ decreases, indicat-

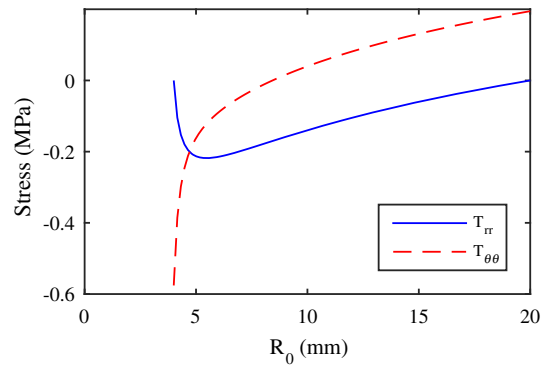


Fig. 8 Radial and circumferential stress for homogeneous planar growth. Equations (22) are solved with stress-free boundary conditions, and the radial, T_{rr} , and circumferential, $T_{\theta\theta}$, stresses are plotted as functions of position. We take $\mu = 0.2$ and $\lambda = 1$ with reference variables: $A = 4$ mm, $a_R = 4.4$ mm, and $B = 20$ mm. The growth components are $\gamma_r = 1.6$ and $\gamma_\theta = 0.95$ marked by a filled circle in Fig. 7

ing that growth must be anisotropic. This is consistent with the modelling assumptions of Wu and Ben Amar (2015), in which the authors assign $\gamma_\theta < 1$ in order to obtain wound closure. If growth were isotropic, i.e. $\gamma_r = \gamma_\theta$, the configuration of the cylinder would lie in region 4 (along the dotted line) and growth would cause the wound to expand. We also observe that, in the regions of interest, growth creates a compressive radial stress, $T_{rr} < 0$ (see Fig. 8). The growth thus serves to counteract the excessive tension created by contraction. On the other hand, both growth and contraction create a compressive hoop stress near the wound edge. A highly compressive hoop stress can result in circumferential buckling (see Wu and Ben Amar (2015), for example), which could mark the onset of scarring. The effect of contraction and growth is counteracted by the fact that the hoop stress is tensile in the recoiled wound; in any case, we leave a stability analysis within this framework for future work.

2.7.1 On geometry

The above analysis highlights the interplay between geometry and mechanics in the wound healing process. In essence, filling a wound in a circular geometry involves a packing problem. In a circular geometry, in order to extend inwards radially the tissue must also vary in the orthogonal direction, undergoing circumferential resorption and/or being put in circumferential compression. In a one-dimensional Cartesian geometry—a “slash wound”—no such geometrical issues exist. The tissue can grow in one Cartesian direction with no change in deformation or stress induced in the orthogonal directions.

Such issues, clearly visible at the tissue level, must be resolved through coordinated activities at the cell level. From a tissue scale modelling viewpoint, such processes are man-

ifest in feedback between mechanical stress and growth. For this, we next turn to heterogeneous growth laws.

2.8 Mechanosensitive growth laws

In general, our growth laws comprise an evolution equation for the growth tensor of the form $\dot{\mathbf{G}} = H(\mathbf{G}, \mathbf{T}, \dots)$ and may incorporate the effects of, for example, biochemistry and temperature. In this work, as we are interested in mechanically stimulated growth, we postulate the form $\dot{\mathbf{G}} = \mathbf{K}(\mathbf{T} - \mathbf{T}^*)\mathbf{G}$, with \mathbf{K} a diagonal tensor so that stress in a given direction induces growth only in that direction. In component form, this is expressed as

$$\frac{\partial \gamma_r}{\partial t} = k(T_{rr} - T_{\text{res}})\gamma_r, \tag{24a}$$

$$\frac{\partial \gamma_\theta}{\partial t} = m(T_{\theta\theta} - T_{\text{res}})\gamma_\theta, \tag{24b}$$

$$\frac{\partial \gamma_z}{\partial t} = nT_{zz}\gamma_z. \tag{24c}$$

In Eqs. (24), k , m , and n are growth rate parameters and T_{res} is the resting residual stress. We note that contraction leads to high radial tension ensuring that $T_{rr} > 0$ and close to the wound edge $T_{\theta\theta} < 0$. This observation suggests that γ_r and γ_θ will naturally evolve towards the ‘‘wound filling’’ location of the phase space in Fig. 7 if k , m , and n are non-negative. To begin with, and for simplicity, we will take $k = m = n$, that is, the sensitivity of the tissue to stress-induced growth is equal in all directions. Initially, no growth occurs so that $\mathbf{G}|_{t=0} = \mathbf{I}$. Equations (24), with $k, m, n > 0$, imply that stress higher than the resting value T_{res} stimulates growth, whereas stress lower than the residual stress causes resorption. This has been observed in wound healing where fibroblast proliferation and collagen synthesis are enhanced in the presence of tension (Kessler et al. 2001) and release of tension can induce apoptosis (Grinnell et al. 1999; Chipev and Simon 2002). Similar assumptions and growth laws have been used in other biological applications such as embryonic wound closure (Taber 2009) and remodelling of arteries (Alford et al. 2008).

2.9 Timescales and recoil dynamics

The recoiled state S_2 is defined to be in mechanical equilibrium. From wound healing data (Bowden et al. 2014), we observe that the recoil of the wound occurs over a period of up to one day. As the dermis moves, this causes friction against the underlying subdermis. Assuming that there is a frictional body force resisting radial motion of the dermis, Eq. (6) can be written as

$$\rho \ddot{\mathbf{x}} - \nabla \cdot \mathbf{T} + q \dot{\mathbf{x}} = \mathbf{0}, \tag{25}$$

where q is a friction coefficient. We now use dimensional arguments to justify whether the time-dependent terms in Eq. (25) are relevant during healing. Let χ denote a characteristic length and t_e , t_d , and t_g the elastic, drag, and growth timescales, respectively. From Eqs. (7) and (8), we deduce the Cauchy stress tensor scales with the shear elastic modulus, μ . The elastic timescale can be determined by balancing the first two terms in Eq. (25), giving $t_e = (\rho \chi^2 / \mu)^{1/2}$.

The healing of the wound occurs on the growth timescale, which is in the order of days (Ghosh et al. 2007). Typical values for the tissue density, $10^{-6} \text{ kg mm}^{-3}$, shear elastic modulus, 0.2 MPa (see Sect. 2.5), and characteristic length, 4 mm, reveal that $t_e \approx \mathcal{O}(10^{-4})$ seconds. Unsurprisingly, $t_e \ll t_g$ and it is appropriate to neglect inertial terms in Eq. (25).

Balancing the second and third terms in Eq. (25) gives a drag timescale of $t_d = q \chi^2 / \mu$. The drag timescale sets the time of wound recoil, which is in the order of hours. This gives $q \approx \mathcal{O}(10^{-3}) \text{ MPa-days-mm}^{-2}$. Once the recoil is complete, the tissue velocity is much slower, and the drag plays a negligible role, i.e. the tissue is essentially in mechanical equilibrium during the growth and contraction phase.

2.10 Contraction

We model wound contraction by prescribing the radial stress at the inner boundary such that

$$T_{rr}|_{r=a} = f_c. \tag{26}$$

In practice, contraction is achieved by fibroblasts which migrate into the tissue and localise around the wound edge. For simplicity, we represent the contractile activity of the fibroblasts as

$$f_c(t) = f a(t) \mathcal{H}(t; t_c, t_m), \tag{27}$$

where f is the contraction coefficient, a is the wound radius, and \mathcal{H} is a linear switch function, parameterised by t_c and t_m , given by

$$\mathcal{H}(t) = \begin{cases} 0 & \text{for } t < t_c \\ \frac{t-t_c}{t_m-t_c} & \text{for } t_c < t < t_m \\ 1 & \text{for } t > t_m. \end{cases} \tag{28}$$

The switch function approximates the time taken for fibroblasts to migrate to the wound edge and begin contracting the tissue. Contraction begins approximately 2 days post-wounding and attains its maximal value approximately 5–14 days after injury (Monaco and Lawrence 2003). In Eq. (28), t_c is the time at which fibroblasts start to localise around the margin and t_m is the time at which the fibroblasts exert their maximum contractile effect.

2.11 The full model

For completeness, we now state the full model, in terms of the independent variables R_0 and t :

$$\frac{\partial r}{\partial R_0} = \gamma_r \gamma_\theta \gamma_z \frac{R_0}{\lambda r}, \quad (29a)$$

$$\frac{\partial T_{rr}}{\partial R_0} = \frac{\gamma_r \gamma_\theta \gamma_z R_0}{\lambda r} \left[\frac{\alpha \hat{W}_\alpha}{r} + q \frac{\partial r}{\partial t} \right], \quad (29b)$$

$$T_{\theta\theta} = T_{rr} + \alpha \hat{W}_\alpha, \quad (29c)$$

$$T_{zz} = T_{rr} + \lambda \hat{W}_\lambda, \quad (29d)$$

$$\frac{\partial \gamma_r}{\partial t} = \begin{cases} 0 & \text{for } t \leq t_R \\ k(T_{rr} - T_{\text{res}})\gamma_r & \text{for } t > t_R \end{cases}, \quad (29e)$$

$$\frac{\partial \gamma_\theta}{\partial t} = \begin{cases} 0 & \text{for } t \leq t_R \\ m(T_{\theta\theta} - T_{\text{res}})\gamma_\theta & \text{for } t > t_R \end{cases}, \quad (29f)$$

$$\frac{\partial \gamma_z}{\partial t} = \begin{cases} 0 & \text{for } t \leq t_R \\ nT_{zz}\gamma_z & \text{for } t > t_R \end{cases}, \quad (29g)$$

In Eqs. (29), $t = t_R$ is the time at which the wound has fully recoiled. The recoil phase occurs in the order of hours, ending before growth and contraction begin ($t_R < t_c$). The boundary conditions are given by

$$T_{rr}(A_0, t) = f a(t) \mathcal{H}(t) \quad \text{and} \quad T_{rr}(B_0, t) = T_{\text{res}}, \quad (29h)$$

$$r(A_0, t) = a(t), \quad (29i)$$

$$N_z(t) = \frac{2\pi}{\lambda(t)} \int_{A_0}^{B_0} \gamma_r \gamma_\theta \gamma_z T_{zz} R_0 \, dR_0 \equiv \eta(1 - \lambda(t)), \quad (29j)$$

where the two extra boundary conditions (Eqs. 29i and 29j) are used to determine the time-dependent unknowns $a(t)$ and $\lambda(t)$. Note that the axial boundary condition (Eq. 29j) is of the form of a spring axial load, which we use to model the resistance of the epidermal layer to axial deformation of the underlying dermal layer. The initial conditions for the components of the growth tensor are given by

$$\gamma_r(R_0, 0) = 1, \quad \gamma_\theta(R_0, 0) = 1, \quad \text{and} \quad \gamma_z(R_0, 0) = 1. \quad (29k)$$

Also, \hat{W} is an auxiliary strain-energy function of only two variables, using incompressibility:

$$\hat{W}(\alpha, \lambda) = \frac{\mu}{2} \left(\frac{\gamma_z^2}{\alpha^2 \lambda^2} + \alpha^2 + \frac{\lambda^2}{\gamma_z^2} - 3 \right). \quad (29l)$$

3 Results

3.1 Numerical implementation

Equations (29) were solved numerically in MATLAB. All dependent variables are stored as functions of R_0 with spatial

discretisation $dx = 0.1$. For each time increment ($dt = 0.05$ days), the growth in Eqs. (29e)–(29g) was updated via a forward Euler scheme (Press et al. 1994). The integral boundary condition in Eq. (29j) was rewritten as a differential equation by letting

$$\frac{\partial I}{\partial R_0} = \gamma_r \gamma_\theta \gamma_z T_{zz} R_0, \quad (30a)$$

with

$$I(B_0) = \frac{N_z}{2\pi} \quad \text{and} \quad I(A_0) = 0. \quad (30b)$$

The radial deformation and radial stress were then determined using the boundary value problem solver `bvp4c` for a system of three differential equations given by Eqs. (29a), (29b), and (30a) subject to boundary conditions in Eqs. (29h), (29i), and (30b). The unknowns a and λ were included in the boundary value problem solver as free parameters which were determined, for each time increment, by prescribing the two extra boundary conditions.

3.2 Model behaviour

In this section, we present typical model solutions, obtained using the parameter values stated in Table 1. These either are taken from the biological literature or were estimated by matching model behaviour to previous healing curves (Bowden et al. 2014).

The plot of the dermal wound radius, $a(t)$, presented in Fig. 9 reveals three distinct phases of healing. During the first phase, which lasts for approximately two days, the wound retracts to a radius 110% of its initial size as a result of the residual tension in the surrounding tissue and the wound radius plateaus before growth and contraction are activated. During the second phase ($2 < t < 14$ days), the wound radius decreases rapidly due to contraction at the wound edge and proliferation of the surrounding tissue. At later times ($t > 14$ days), as the wound radius decreases, contraction slows down, since it is proportional to the wound radius. As a result of the mechanosensitive properties of the tissue, growth also slows down and the wound radius begins to plateau. We note that the healing curve is qualitatively similar to experimental data (McGrath and Simon 1983; Bowden et al. 2014).

In Fig. 10, we plot the corresponding growth and stress components, associated with the simulation in Fig. 9, as functions of the undeformed radius R_0 at days 2, 14, and 25. As expected, since growth is mechanosensitive, with the growth rates in Eqs. (24) depending linearly on the stress, the growth and stress profiles are qualitatively similar with the radial stress and growth increasing over time as the contraction force increases. Contraction reaches a maximum at day 14, and we observe that the radial stress at day 25 is

Table 1 Model parameters

Parameter	Physical interpretation	Units	Physical range	References	Default
k	Radial growth	$\text{MPa}^{-1} \text{ days}^{-1}$	$k > 0$		0.2
m	Circumferential growth	$\text{MPa}^{-1} \text{ days}^{-1}$	$m > 0$		0.2 (0.1)
n	Axial growth	$\text{MPa}^{-1} \text{ days}^{-1}$	$n > 0$		0.2 (0.1)
f	Contraction	MPa mm^{-1}	$0 < f < 1.325$	Uhal et al. (1998) and Wrobel et al. (2002)	0.2
t_c	Contraction begins	days	2 – 5	Monaco and Lawrence (2003)	2
t_m	Maximum contraction	days	5 – 14	Monaco and Lawrence (2003)	14
q	Friction	MPa days mm^{-2}	$q = \mathcal{O}(10^{-3})$	Estimated (see Sect. 2.9)	0.002
μ	Shear elastic modulus	MPa	$0.02 < \mu < 0.52$	Estimated (see Sect. 2.5)	0.2
N_z	Axial load	N			
η	Load coefficient	N			10
A	Initial wound radius	mm	$A > 0$	McGrath and Simon (1983)	4
a_R	Recoiled wound radius	mm	$a_R > A$	McGrath and Simon (1983)	4.4
B	Domain size	mm	$B > a_R$	Estimated (see Sect. 2.4)	20
L	Tissue thickness	mm	$L > 0$	Bowden et al. (2014)	0.1

Table summarising the parameters that appear in our mathematical model along with their physical interpretation, default values, and supporting references. Values in brackets are adopted after Sect. 3.4

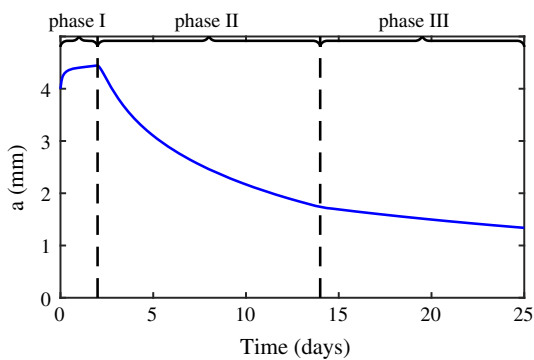


Fig. 9 Typical model solution with healing phases. Equations (29) are solved numerically, and the wound radius $a(t)$ is plotted as a function of time. Reference variables and parameters are specified using the default values in Table 1. The healing curve can be separated into three distinct phases representing the initial recoil, a proliferative and contracting phase, and finally the rate of closure slows down as contraction and growth decrease

less than that on day 14. As expected, radial growth and stress are larger closer to the wound edge. The dermis is in compression in the circumferential and axial directions and, as a consequence, material is resorbed in these directions. With $\gamma_\theta < 1 < \gamma_r$, we are in a regime associated with normal healing (see Sect. 2.7), for which the wound radius decreases while the outer radius remains approximately constant. We interpret the removal of tissue from the circumferential direction ($\gamma_\theta < 1$) as tissue remodelling—the net change in volume is locally given by $(\det \mathbf{G} - 1)$, which is positive.

3.3 Sensitivity of final wound radius to model parameters

Ultimately, we are interested in the time to closure and the quality and mechanical properties of the healed tissue. In Fig. 11, we show how the wound radius at day 25 changes as we vary the default model parameters by $\pm 10\%$, one parameter at a time. We observe that increasing the radial growth sensitivity k causes the wound radius to decrease. Increasing the rate of circumferential absorption (since the circumferential stress is negative) accelerates wound closure in a manner similar to that seen by increasing the contraction coefficient. Interestingly, circumferential resorption has previously been used as a contractile mechanism in a model of epidermal wound closure (Wu and Ben Amar 2015). The effect of axial growth on the wound radius is negligible, and as expected, increasing tissue stiffness has a detrimental effect on wound closure, since a stiffer tissue will deform less when subject to a given force.

3.4 Anisotropic growth rate constants

We expect that, as the wound heals, the dermal tissue experiences a net gain in material. In Figure 12, we demonstrate the effect on the net change in volume on day 25 as we vary the growth rate parameters by $\pm 50\%$. We find that the default set of parameters (with all growth rates equal) results in a net loss of material. In order for the wound to heal with a net gain in material, we require a higher radial than circumferential ($k > m$) growth rate. This anisotropy in growth rate essen-

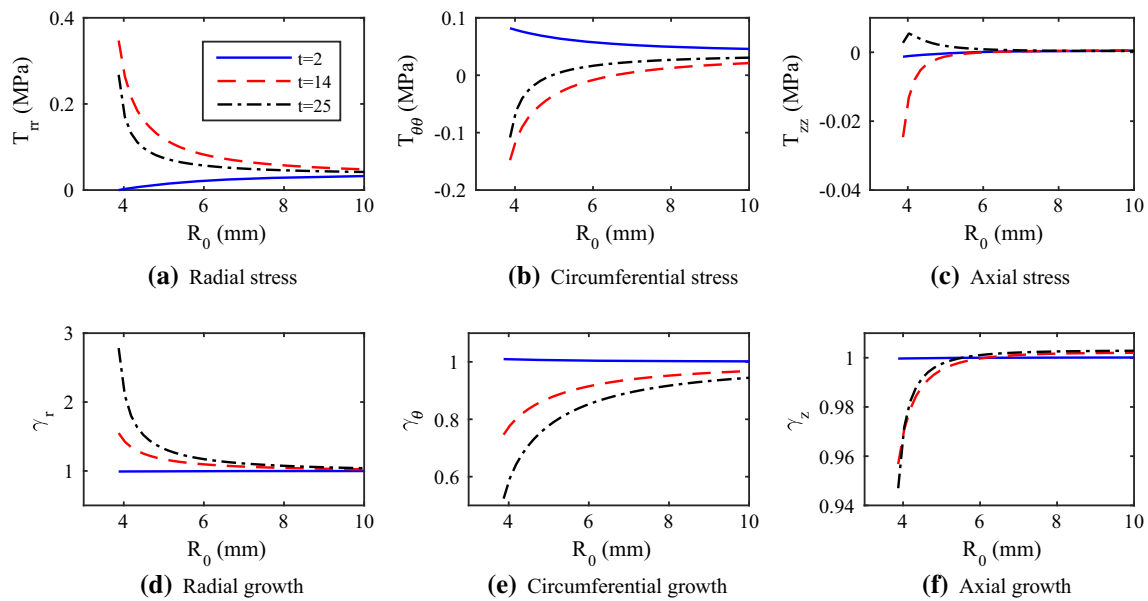


Fig. 10 Typical model solution for the stress and growth. Equations (29) are solved numerically. **a** The radial stress T_{rr} , **b** the circumferential stress $T_{\theta\theta}$, **c** the axial stress T_{zz} , **d** the radial growth γ_r , **e** the circumferential growth γ_θ , and **f** the axial growth γ_z are plotted as functions of position at 2 (solid line), 14 (dashed line), and 25

(dotted dashed line) days. Reference variables and parameters are specified using the default values in Table 1. The radial stress is higher closer to the wound edge, resulting in higher radial growth there. The tissue is in compression circumferentially and axially, resulting in resorption of material in these directions

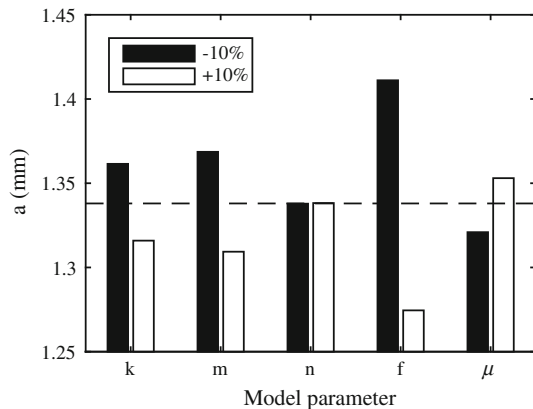


Fig. 11 Effect of model parameters on final wound radius. Equations (29) are solved numerically. Each model parameter is varied by $\pm 10\%$ of its default value, and the wound radius at day 25 is recorded. The dashed line indicates the wound radius when all parameters are fixed at their default values. All reference variables and parameters are specified using the default values in Table 1. Increasing the radial and circumferential growth parameters, k and m , and the contraction coefficient, f , decreases the wound radius at day 25. Increasing the axial growth parameter, n , has negligible effect on the wound radius at day 25. Increasing the tissue stiffness, μ , decreases the wound radius at day 25

tially requires that a cell can sense the radial direction; in fact, this may not be so surprising. Fibroblast cells migrate radially in response to chemical growth factor gradients (Pierce et al. 1989; Chung et al. 2001), and hence, a directional bias for radial growth is feasible. Therefore, we take $k > m$ in

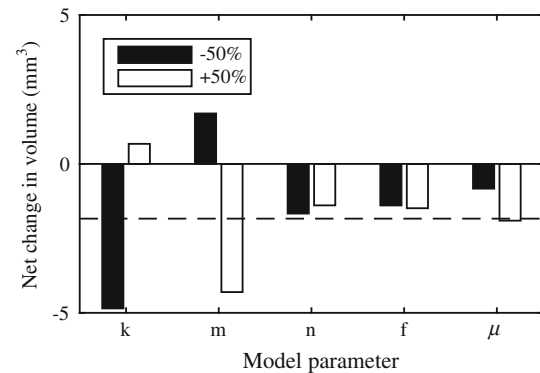


Fig. 12 Effect of model parameters on net change in volume. Equations (29) are solved numerically. Each parameter is varied by $\pm 50\%$ of its default value, and the net change in volume at day 25 is recorded. The dashed line indicates the net change in volume when all parameters are fixed at their default values. All reference variables and parameters are specified using the default values in Table 1. For the given default parameters, there is a net loss in material. A net gain in material can be achieved by either increasing the radial growth rate k or decreasing the circumferential growth rate m

the remainder of this work so as to incorporate a radial bias ($k = 0.2$, $m = 0.1$, $n = 0.1$).

3.5 Remodelling after closure

We anticipate that, after the wound has closed, the dermal tissue remodels to its natural state of residual stress. The formation of granulation tissue in the wound space (later

remodelled into scar tissue) prevents the dermis from closing completely. Therefore, there is a point at which the dermal edge halts. The mechanism by which this occurs is not known, but could involve a combination of contraction ceasing (due to inactivation of fibroblasts), the radial stress reaching a threshold value and the granulation tissue in the wound space acting as a physical barrier, preventing further inward movement of the dermis. The questions we consider are whether the halted tissue will reach an equilibrium state, returning to the base residual stress and, if so, how long the remodelling will take.

We simulate the remodelling period of the dermal tissue by halting the wound edge at some point $t = T$. We choose $T = 25$ days as a representative time by which the granulation tissue fills the wound space, but note that the stimulus that halts movement of the dermal edge could easily be modified to account for other effects.

We solve Eqs. (29) for $0 \leq t \leq T$. For $t > T$, we switch the boundary conditions from the fixed load specified in Eqs. (29h)–(29j) to a fixed displacement so that

$$r(A_0, t) = a(T), \quad r(B_0, t) = b(T), \quad \lambda(t) = \lambda(T). \quad (31)$$

This fixes the deformation, preventing the wound from closing further. Due to incompressibility and a fixed deformation, there can be no net change in material so that $\frac{\partial}{\partial t}(\det(\mathbf{G})) = 0$. We therefore have the following system for $t > T$ (=25 days):

$$\frac{\partial \gamma_r}{\partial t} = k(T_{rr} - T_{res})\gamma_r, \quad (32a)$$

$$\frac{\partial \gamma_\theta}{\partial t} = m(T_{\theta\theta} - T_{res})\gamma_\theta, \quad (32b)$$

$$\frac{\partial \gamma_z}{\partial t} = nT_{zz}\gamma_z, \quad (32c)$$

$$T_{\theta\theta} = T_{rr} + \alpha \hat{W}_\alpha, \quad (32d)$$

$$T_{zz} = T_{rr} + \lambda \hat{W}_\lambda, \quad (32e)$$

$$\frac{\partial}{\partial t}(\gamma_r \gamma_\theta \gamma_z) = 0. \quad (32f)$$

Expanding Eq. (32f) and inserting Eqs. (32a)–(32c) yields a relationship for the stress in terms of the growth and the strain

$$T_{rr} = \frac{(k + m)T_{res} - m\alpha \hat{W}_\alpha - n\lambda \hat{W}_\lambda}{k + m + n}, \quad (33a)$$

$$T_{\theta\theta} = T_{rr} + \alpha \hat{W}_\alpha, \quad (33b)$$

$$T_{zz} = T_{rr} + \lambda \hat{W}_\lambda, \quad (33c)$$

where \hat{W} is defined in Eq. (29l). The components of the growth tensor satisfy Eqs. (32a)–(32c), and the stress is updated according to Eqs. (33).

In Fig. 13a–c, we plot the components of the stress tensor at days 25, 50, and 100. At day 25, we observe a large radial tension at the wound edge, with circumferential and axial compression of similar magnitude. Over the remodelling period, these profiles relax to a steady state with the stress returning to the isotropic planar stress state $T_{rr} = T_{\theta\theta} = T_{res}$, $T_{zz} = 0$. In Fig. 13d, e, the components of the stress and growth tensors are plotted as functions of position at day 200, after the system has reached steady state. Figure 13f shows how the spatial averages of the components of the growth tensor evolve over time. We find that growth has slowed down by day 50 and that by day 100 the remodelling phase is essentially complete.

3.5.1 Sensitivity of remodelling time to model parameters

We now investigate how the duration of the remodelling phase changes as we vary parameters associated with the growth and tissue stiffness. The results are given as a bar graph of the time taken for the tissue to reach a steady state in Fig. 14. Steady state is defined as²

$$\frac{\partial \gamma_r}{\partial t} = \frac{\partial \gamma_\theta}{\partial t} = \frac{\partial \gamma_z}{\partial t} = 0. \quad (34)$$

In order to make a reliable comparison, the model parameters are not changed for the first 25 days of healing. After day 25, when the tissue begins to remodel, each model parameter is varied by $\pm 10\%$ of its default value. We observe that the tissue stiffness has the greatest effect on the remodelling time, such that as μ is increased by 10%, the time taken for the tissue to reach steady state is reduced by approximately 10 days. For the remaining model parameters tested, the remodelling time is between 120 and 150 days. Comparing the sensitivity of the remodelling time to the model parameters with that of the final wound radius, we observe some significant differences. In Fig. 11, the radial and circumferential growth parameters had a similar effect on the final wound radius; however, in Fig. 14 circumferential growth has a much greater effect than radial growth. This may be due to the degree of radial versus circumferential stress the tissue needs to recover. We observe in Fig. 13a, b that at day 25 the radial and circumferential stresses at the wound edge are 0.2451 and -0.2621 MPa, respectively. With a positive resting stress ($T_{res} = 0.0376$ MPa), the growth rates in Eqs. (24) imply that the circumferential growth rate dominates the radial growth rate. Surprisingly, varying the axial growth rate, which had negligible effect on

² Numerically, we define steady state to be such that each $\frac{\partial \gamma_i}{\partial t}$ is below a positive threshold value close to zero. For the simulations in Fig. 14, the threshold was taken to be 10^{-5} .

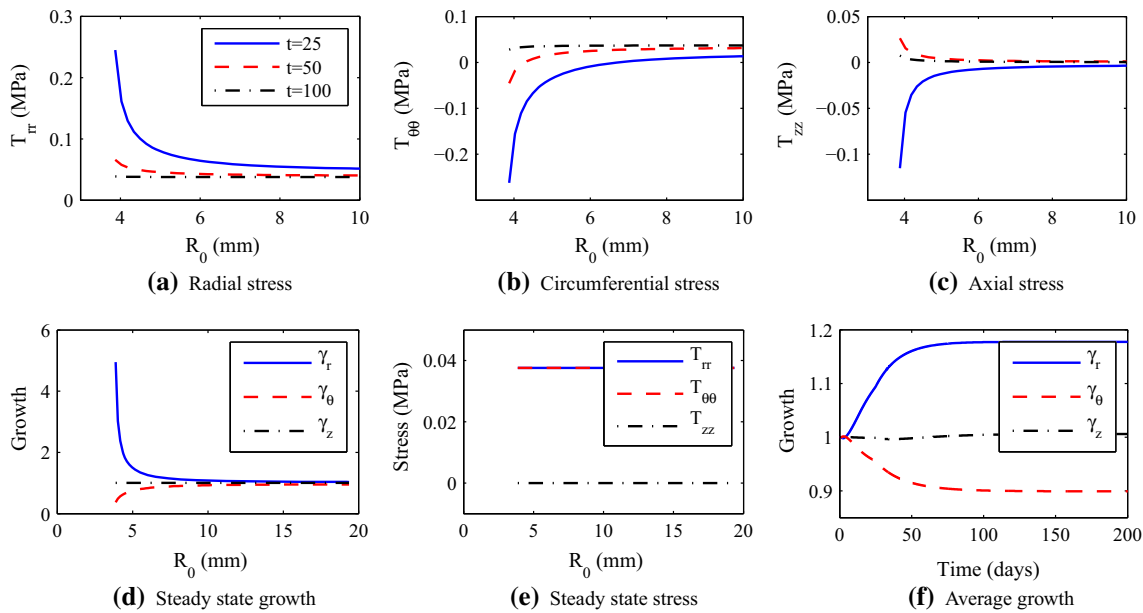


Fig. 13 Remodelling of the dermal tissue. Equations (29) are solved numerically for $0 < t < 25$. At $t = 25$, the position of the wound edge is fixed by switching the boundary condition from a fixed load (Eqs. 29h–29j) to a fixed displacement specified by Eq. (31). **a** The radial stress T_{rr} , **b** the circumferential stress $T_{\theta\theta}$, and **c** the axial stress T_{zz} are plotted as functions of position at 25, 50, and 100 days. **d** The

radial, circumferential, and axial growth and **e** stress are plotted as functions of position at 200 days. **f** The average radial, circumferential, and axial growth are plotted as functions of time. Reference variables and parameters are specified using the default values in Table 1. The growth reaches a steady state by approximately day 100, and the stress returns to the isotropic planar stress T^*

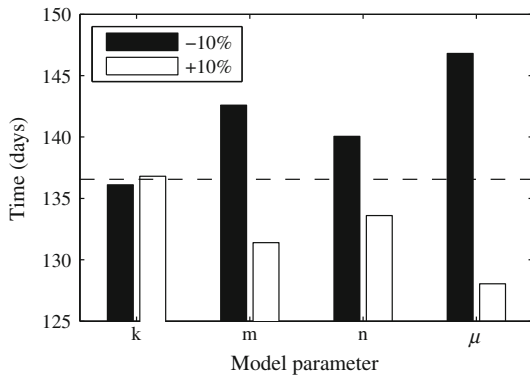


Fig. 14 Effect of model parameters on remodelling time. Equations (29) are solved numerically for $0 < t < 25$. At $t = 25$, the position of the wound edge is fixed by switching the boundary condition from a fixed load (Eqs. 29h–29j) to a fixed displacement specified by Eq. (31). During the remodelling phase, each model parameter is varied by $\pm 10\%$ of its default value and the time taken to reach steady state is recorded. The dashed line indicates the remodelling time when all parameters are fixed at their default values. Reference variables and parameters are specified using the default values in Table 1

the healing curve, has a significant effect on the remodelling time. We postulate that this is due to the fixed axial deformation³.

³ To test this, we ran simulations where the axial deformation was not fixed according to $\lambda(t) = \lambda(T)$, but instead satisfied the spring condition in Eq. (29j). In this case, the sensitivity of the remodelling time to the axial growth parameter was significantly lower than that presented in Fig. 14.

3.5.2 Steady state solution

Figure 13 shows that, for the default parameter values in Table 1, the stress reaches a steady state for which $T = T^*$. The growth laws in Eqs. (24) ensure that this is the only steady state solution. A natural question is whether the growth profile (for example, that shown in Fig. 13d) needed to reach this state is unique. At steady state, we have

$$\frac{\partial r}{\partial R_0} = \frac{\gamma_\theta \gamma_r \gamma_z R_0}{\lambda r} \tag{35a}$$

$$T_{\theta\theta} = T_{rr} + \alpha \hat{W}_\alpha \tag{35b}$$

$$T_{zz} = T_{rr} + \lambda \hat{W}_\lambda. \tag{35c}$$

For a fixed deformation with $T = T^*$, solving Eqs. (35) for the components of the growth tensor gives

$$\gamma_\theta = \sqrt{\frac{\lambda}{\gamma_z}} \frac{r}{R_0} \tag{36a}$$

$$\gamma_r = \sqrt{\frac{\lambda}{\gamma_z}} \frac{\partial r}{\partial R_0} \tag{36b}$$

$$\left(\frac{\gamma_z}{\lambda}\right)^3 - \frac{T_{res}}{\mu} \left(\frac{\gamma_z}{\lambda}\right)^2 - 1 = 0. \tag{36c}$$

Since $\lambda, \mu > 0$, Eq. (36c) has only one real root for $T_{\text{res}} > -\left(\frac{27}{4}\right)^{\frac{1}{3}}\mu$ given by

$$\gamma_z = \left(\frac{C}{6\mu} + \frac{2T_{\text{res}}^2}{3\mu C} + \frac{T_{\text{res}}}{3\mu} \right) \lambda, \tag{37}$$

where $C = \left[12\mu^2 \sqrt{\frac{12T_{\text{res}}^3 + 81\mu^3}{\mu}} + 8T_{\text{res}}^3 + 108\mu^3 \right]^{\frac{1}{3}}$

and three distinct real roots for $T_{\text{res}} < -\left(\frac{27}{4}\right)^{\frac{1}{3}}\mu$. That is, if the residual stress is negative (i.e. the skin is in compression before wounding) and large enough, there are three possible choices for γ_z at steady state. Therefore, the roots of Eq. (36c) depend on the residual stress where there is always one positive root. For $T_{\text{res}} < -\left(\frac{27}{4}\right)^{\frac{1}{3}}\mu$, there is a fold bifurcation with two extra roots; however, these are both negative. The qualitative behaviour of this bifurcation does not change for different values of μ and λ .

Since the growth profiles of γ_r and γ_θ depend on γ_z and we require $\gamma_z > 0$ in Eqs. (36) for physiologically real solutions, we conclude that the steady state profiles of the growth components in Fig. 13d, associated with $T = T^*$ and $T_{\text{res}} > 0$, are unique.

3.6 Model experiments

The model we have developed provides a framework for investigating wound healing from a mechanical point of view. This can have particular value in the context of experiments in which the mechanical environment is explicitly altered. In this section, we consider two such scenarios, rewounding and the application of pressure during healing.

3.6.1 Rewounding

The mechanical model gives access to the stress state in the tissue at any point or time. It is difficult to access the stress profile experimentally, but the effect of stress can clearly be seen when it is relieved. Rewounding, i.e. recutting a wound in the same location, provides one means of accessing the mechanical state. In the same manner as the degree of recoil upon initial wounding can be used to measure the residual tension in the healthy skin, measuring the degree of recoil upon rewounding gives a measure of the stress state in the skin during the healing process. Similar experiments have previously been used to determine whether the embryonic ‘‘purse-string’’ mechanism is in tension (Davidson et al. 2002).

A hypothetical rewounding experiment also provides a means of calibrating our model. We have found that different balances of growth and contraction can generate

similar healing profiles. Alternatively, wound closure can also be achieved with conceptually opposing growth laws and mechanical boundary conditions (Taber 2009). Currently, most experimental data comprise time series of averaged wound areas. With such data, it is not possible to distinguish such cases: additional information about the stress during healing is needed to calibrate the model and compare alternative hypotheses. In theory, a rewounding experiment could be repeated at regular intervals during healing to give a time series of spatially averaged stress measurements.

Here, we simulate rewounding, using the model to predict the retraction of a wound in response to a second injury. By varying the radial growth and contraction coefficients, k and f , we compare two cases: (a) healing with high growth and low contraction and (b) healing with low growth and high contraction. While the evolution of the wound radius in each case is similar (see Fig. 15), the stress generated in the tissue differs markedly. When the rate of contraction is high, the stress at the wound edge is much greater than when the contraction rate is small (results not shown). In the absence of measurements of the stress profile, making a new wound and recording the retracted area would enable us to estimate the tension in the skin and to determine whether contraction or growth dominates healing. The retraction of the second injury in Fig. 15b, when the dermal tissue is subject to low growth and high contraction, is much greater than that in Fig. 15a where the dermal tissue is subject to higher growth and lower contraction.

3.6.2 Pressure treatments

Pressure therapy involves the application of pressure to control wound healing. The most common application of pressure therapy for the management of hypertrophic scars is via pressure bandages (Kischer 1975). Despite their widespread use, the mechanism by which pressure bandages improve healing is not fully understood and the clinical effectiveness of this non-invasive therapy remains to be scientifically proven (Anzarut et al. 2009). It has been suggested that mechanical pressure induces a hypoxic atmosphere resulting in death of fibroblasts and therefore reduced tissue synthesis (Kischer 1975). Alternatively, mechanical pressure may inhibit the activity of fibroblasts by reducing the rate at which they secrete TGF β , a growth factor which stimulates fibroblasts to contract and produce tissue (Martin 1997).

As well as the application of pressure to retard the proliferative activity of fibroblasts during healing, negative pressure wound therapy (NPWT), or vacuum-assisted closure (VAC), is used to stimulate tissue regeneration in non-healing wounds. NPWT and VAC have been shown to increase blood flow and granulation tissue formation, to decrease bacteria, and to stimulate tissue synthesis through increased mechanical tension (Mendez-Eastman 2001; Huang et al. 2014).

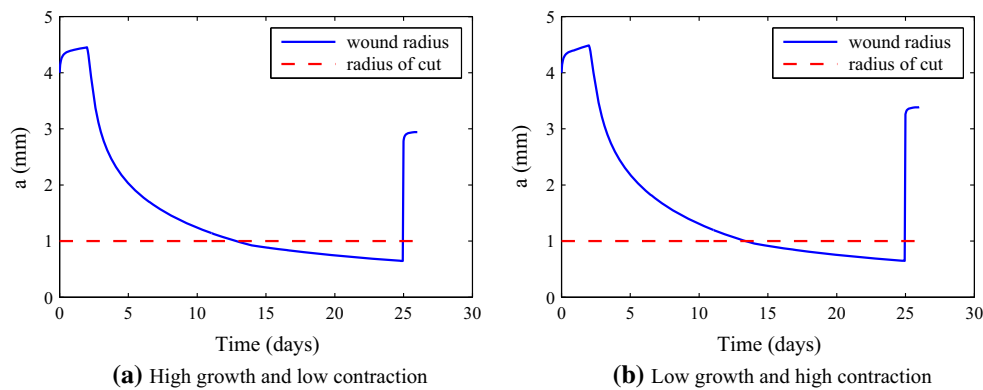


Fig. 15 Predicted outcome of rewounding experiments. Equations (29) are solved numerically, and at $t = 25$ a wound of radius 1 mm is cut. The wound radius is plotted as a function of time for a

high growth and low contraction ($k = 0.8$, $f = 0.3$), **b** *low growth and high contraction* ($k = 0.1$, $f = 0.5$). All other reference variables and parameters are specified using the default values in Table 1

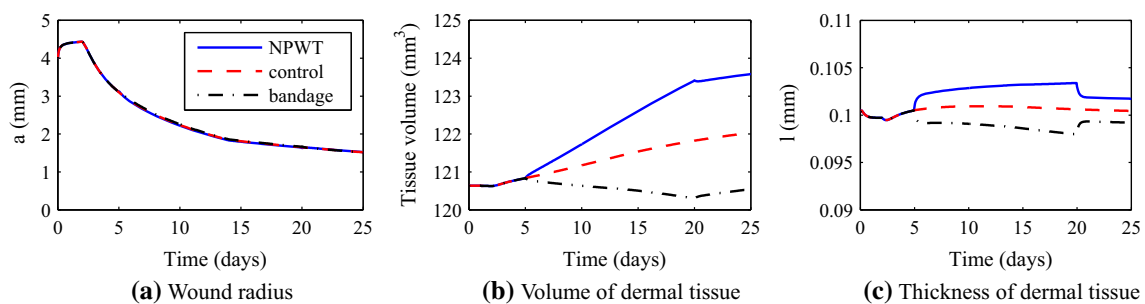


Fig. 16 Effect of axial load on the healing dermis. Equations (29) are solved numerically. From day 5–20, axial load is assigned for NPWT ($N_z = 10$ N, —), control ($N_z = 0$ N, - -), and pressure bandage ($N_z = -10$ N, · ·). **a** The wound radius $a(t)$, **b** the total tissue vol-

ume, and **c** the tissue thickness $l(t)$ are plotted as functions of time. Reference variables and parameters are specified using the default values in Table 1

The pressure needed for effective treatment is unknown, although values in the range 9–90 mmHg (0.001–0.01 MPa) have been reported (Giele et al. 1997). Alternatively, NPWT tends to generate up to 125 mmHg of suction in the wound area (approximately 0.017 MPa). In this section, we use our mechanical model to investigate the effects of applying pressure to the surrounding dermal tissue during healing. Using Eq. (29j) with a modelling domain of radius 20 mm, the pressures discussed here can be approximated by axial loads ranging from -12.5 to 21.5 N.

We simulate treatment for a period of 15 days. The wound begins to heal load-free ($N_z = 0$ N). On day 5, pressure is applied by assigning a nonzero axial load ($N_z = 10$ or $N_z = -10$ N). Pressure is released on day 20, and the wound continues to heal load-free until day 25.

In Fig. 16a, we show how the wound radius responds to different axial loads. We observe that the effect of axial load on the wound radius is negligible. However, Fig. 16b reveals that the tissue volume is greatly affected by applying a constant axial load. When the load is positive, for example corresponding to NPWT, the tissue mass added during the

treatment period is 3 times greater than in the control case. When the load is negative, for example in the application of a pressure bandage, there is a loss in total tissue volume. In Fig. 16c, the tissue thickness is plotted as a function of time. We observe that, although the changes in volume do not affect the wound radius, they contribute to the thickness of the tissue. We also observe that when the load is released, the thickness of the dermal tissue returns to a value closer to the control case, but there is still a noticeable difference, most likely due to the difference in tissue volume observed in Fig. 16b. These results suggest that although applying an axial load has negligible effect on the healing curve, it could be used to control the total amount of tissue produced in the surrounding dermis during healing.

4 Discussion

In this paper, we have developed a mechanical model of dermal wound healing in which closure is driven by contraction of the wound edge and mechanically induced volumetric

growth. Our first step was to establish the degree of residual tension in the pre-wounded tissue by analysing the recoil that is observed after circular punch biopsies in mice. Volumetric tissue growth was motivated by the unrealistically high stresses that would be generated in the tissue surrounding the wound area if healing were to occur through contraction alone. A simple analysis of homogeneous growth revealed that normal healing should be characterised by anisotropic growth, with the addition of material in the radial direction and removal of material in the circumferential direction. In the full model, we have postulated simple mechanosensitive growth laws that enable us to isolate the effects of such anisotropy during healing simulations.

Typical solutions of the model revealed three distinct phases of healing. Initially, the wound retracts and the radius plateaus due to no growth or contraction (up to 2 days). The wound radius then decreases over approximately 14 days as a result of contraction and mechanosensitive growth. Finally, contraction and mechanosensitive growth slow down. Over a much longer time period (approximately 100 days), the dermal tissue remodels, returning to its homeostatic resting stress. We show that there is only one steady state for the stress, corresponding to $T = T^*$, with one associated nonnegative steady state growth profile. The system takes approximately 120–150 days to remodel, depending on the choice of model parameters.

Fundamental difficulties in linking modelling and experimental efforts in wound healing relate to overparameterisation of the mathematical models and the technical difficulty associated with obtaining suitable experimental data for model validation. While our modelling framework neglects many features of the wound healing process, such as an explicit description of fibroblast activity, it has the advantage of characterising wound healing of a nonlinear elastic tissue in a simple manner and with a small number of parameters. We have shown that the model captures well the qualitative features of healing curves obtained in mice. The problem is that such features are not unique, even while varying a set of only 4 free parameters. For instance, we find that if one is only tracking the wound radius over time, two different parameter regimes—one with high growth and low contraction, and one with low growth and high contraction—can both produce the same healing curve for the wound radius. However, such cases can be distinguished if additional mechanical information is available. We have simulated rewounding experiments, in which the wound is recut before it is fully healed. The degree of recoil can be used to distinguish between cases and calibrate the model. Such experiments can also provide useful information about the mechanical state of the healing tissue and the mechanosensitivity of the growing tissue.

Our framework is also well suited to investigate pressure treatments. By applying an axial load to the healing dermis,

we observed that loads reported in the literature do not change the behaviour of the healing curve but can have a significant effect on the total volume of tissue produced during healing. Therefore, if the dermis is hyperproliferative during healing, applying pressure to the area can normalise the overall tissue volume. Similarly, if the dermis is under-proliferative, applying suction can normalise the volume of tissue produced.

We have considered circular wounds, as arising, for example, from a circular punch biopsy. We have, therefore, restricted our modelling to a cylindrical geometry. Assuming that the tissue is homogeneous, we showed that residual stress in the unwounded skin is isotropic. Under this assumption, a circular wound will remain circular when cut and, hence, we have restricted attention to symmetric deformations. A stability analysis would be straightforward and could provide information on scarring; see, for instance, [Wu and Ben Amar \(2015\)](#). We employed the simplest isotropic constitutive equation for a hyperelastic material (neo-Hookean) allowing for analytical progress. Other constitutive equations, such as Mooney–Rivlin or Fung, could easily be incorporated. However, considering a more realistic anisotropic strain-energy, such as that determined by [Annaidh et al. \(2012\)](#), would be much more complicated and the simplicity and analytical power of the proposed model would be lost.

Due to the lack of experimental data on wound healing in humans, we have presented results using parameter values and tissue dimensions obtained from experiments in mice. Given accurate experimental data, the parameters in the model could be adapted to simulate healing in humans.

The mechanosensitive growth laws in our model are similar to those used in a model of embryonic wound healing ([Taber 2009](#)). In embryonic wound healing, contraction is generated by a “purse-string” ([Martin and Lewis 1992](#); [Davidson et al. 2002](#)), modelled by circumferential resorption at the wound edge in both [Taber \(2009\)](#) and [Wu and Ben Amar \(2015\)](#). By combining experimental and computational approaches, [Wyczalkowski et al. \(2013\)](#) investigate in more detail possible mechanisms of the “purse-string”. It has been shown that the contraction mechanism in dermal wound closure does not proceed via a “purse-string” ([Gross et al. 1995](#)) and was therefore not considered in the present study. While the growth profiles in [Fig. 10](#) are qualitatively similar to those found in [Taber \(2009\)](#), there are fundamental differences. Taber’s growth laws are formulated with zero net change in volume and feedback such that *compression* relative to the target stress stimulates growth. In comparison, our model has the feedback in the opposite direction (with tension stimulating growth) and a net volumetric growth that serves to counteract the tension due to contraction. The key to such opposing forms is a difference in activity at the wound edge and how this translates to a boundary condition for the mechanics. In the Taber’s model, the wound edge is stress-free and hence, below the resting stress, so that a negative

growth law induces the required radial growth. Here, the contractile force places the wound edge above the resting tension, so that a positive growth law is needed. Nevertheless, that models with contrasting feedback can generate similar healing profiles suggests a clear need for further investigation both on the tissue and on cellular scales. Different modelling approaches will generally have differing mechanical signatures, and experiments such as the rewounding discussed in the present work could be used to discriminate between them.

In order to focus on the mechanical environment in the tissue, we have restricted to mechanically stimulated growth, such that stress greater (less) than the residual stress results in addition (removal) of material. With the growth laws formulated in this manner, growth will not occur unless contraction is active. It is quite likely that basal or chemically stimulated growth occurs in the absence of contraction and we intend to include this in future modelling efforts. Our sensitivity analysis in Sect. 3.4 showed that, to achieve a net gain in material, mechanosensitive growth should have a radial bias. This could be achieved with a growth factor gradient in the radial direction. A natural next step is to couple a mathematical description of fibroblast and growth factor activity to the contraction function and the evolution of growth laws providing a more mechanistic approach to the main processes driving dermal wound closure and the inclusion of chemically stimulated growth. Validation of our model against experimental data is required; for example, the rewounding experiments discussed in this paper are currently underway.

Acknowledgments LGB gratefully acknowledges the UK's Engineering and Physical Sciences Research Council for funding through a studentship at the Systems Biology programme of the University of Oxford's Doctoral Training Centre. The authors thank Dr. P.Y. Liu and Dr. X.T. Wang (Department of Plastic Surgery, Alpert Medical School of Brown University) for valuable discussions.

Conflict of interest The authors declare that they have no conflict of interest.

References

- Alford P, Humphrey J, Taber L (2008) Growth and remodeling in a thick-walled artery model: effects of spatial variations in wall constituents. *Biomech Model Mechanobiol* 7(4):245–62
- Ambrosi D, Mollica F (2004) The role of stress in the growth of a multicell spheroid. *J Math Biol* 48(5):477–99
- Annai A, Bruyère K, Destrade M, Gilchrist M, Maurini C, Otténio M, Saccomandi G (2012) Automated estimation of collagen fibre dispersion in the dermis and its contribution to the anisotropic behaviour of skin. *Ann Biomed Eng* 40(8):1666–78
- Anzarut A, Olson J, Singh P, Rowe B, Tredget E (2009) The effectiveness of pressure garment therapy for the prevention of abnormal scarring after burn injury: a meta-analysis. *J Plast Reconstr Aes* 62(1):77–84
- Bermudez D, Herdrich B, Xu J, Lind R, Beason D, Mitchell M, Soslowsky L, Liechty K (2011) Impaired biomechanical properties of diabetic skin implications in pathogenesis of diabetic wound complications. *Am J Pathol* 178(5):2215–23
- Bowden L, Maini P, Moulton D, Tang J, Wang X, Liu P, Byrne H (2014) An ordinary differential equation model for full thickness wounds and the effects of diabetes. *J Theor Biol* 361:87–100
- Chipev C, Simon M (2002) Phenotypic differences between dermal fibroblasts from different body sites determine their responses to tension and $\text{tgf}\beta 1$. *BMC Dermatol* 2(1):13
- Chung CY, Funamoto S, Firtel R (2001) Signaling pathways controlling cell polarity and chemotaxis. *Trends Biochem Sci* 26(9):557–566
- Ciarletta P, Ben Amar M (2012) Papillary networks in the dermal-epidermal junction of skin: a biomechanical model. *Mech Res Commun* 42:68–76
- Ciarletta P, Foret L, Ben Amar M (2011) The radial growth phase of malignant melanoma: multi-phase modelling, numerical simulations and linear stability analysis. *J R Soc Interface* 8(56):345–368
- Clark R (1988) *The molecular and cellular biology of wound repair*. Plenum, New York
- Cumming B, McElwain D, Upton Z (2010) A mathematical model of wound healing and subsequent scarring. *J R Soc Interface* 7(42):19–34
- Dallon J (2000) Biological implications of a discrete mathematical model for collagen deposition and alignment in dermal wound repair. *Math Med Biol* 17(4):379–393
- Dallon J, Sherratt J, Maini P (1999) Mathematical modelling of extracellular matrix dynamics using discrete cells: fiber orientation and tissue regeneration. *J Theor Biol* 199(4):449–71
- Davidson L, Ezin A, Keller R (2002) Embryonic wound healing by apical contraction and ingression in *xenopus laevis*. *Cell Motil Cytoskeleton* 53(3):163–176
- Diridollou S, Patat F, Gens F, Vaillant L, Black D, Lagarde J, Gall Y, Berson M (2000) In vivo model of the mechanical properties of the human skin under suction. *Skin Res Technol* 6(4):214–221
- Ehrlich H (1988) Wound closure: evidence of cooperation between fibroblasts and collagen matrix. *Exp Cell Res* 177:149–157
- Ehrlich H, Rajaratnam J (1990) Cell locomotion forces versus cell contraction forces for collagen lattice contraction: an in vitro model of wound contraction. *Tissue Cell* 22(4):407–417
- Eringen A (1962) *Nonlinear theory of continuous media*. McGraw-Hill, New York
- Flynn C, Taberner A, Nielsen P (2011) Modeling the mechanical response of in vivo human skin under a rich set of deformations. *Ann Biomed Eng* 39(7):1935–46
- Ghosh K, Pan Z, Guan E, Ge S, Liu Y, Nakamura T, Ren X, Rafailovich M, Clark RAF (2007) Cell adaptation to a physiologically relevant ECM mimic with different viscoelastic properties. *Biomaterials* 28(4):671–679
- Giele H, Liddiard K, Currie K, Wood F (1997) Direct measurement of cutaneous pressures generated by pressure garments. *Burns* 23(2):137–141
- Goriely A, Vandiver R (2010) On the mechanical stability of growing arteries. *IMA J Appl Math* 75(4):549–570
- Goriely A, Moulton D, Vandiver R (2010) Elastic cavitation, tube hollowing, and differential growth in plants and biological tissues. *Europhys Lett* 91(1):18,001
- Grinnell F, Zhu M, Carlson MA, Abrams JM (1999) Release of mechanical tension triggers apoptosis of human fibroblasts in a model of regressing granulation tissue. *Exp Cell Res* 248(2):608–619
- Gross J, Farinelli W, Sadow P, Anderson R, Bruns R (1995) On the mechanism of skin wound “contraction”: a granulation tissue “knockout” with a normal phenotype. *P Natl A Sci USA* 92(13):5982–5986
- Hex N, Bartlett C, Wright D, Taylor M, Varley D (2012) Estimating the current and future costs of type 1 and type 2 diabetes in the UK, including direct health costs and indirect societal and productivity costs. *Diabetic Med* 29(7):855–62

- Huang C, Leavitt T, Bayer L, Orgill D (2014) Effect of negative pressure wound therapy on wound healing. *Curr Prob Surg* 51(7):301–31
- Jacquet E, Josse G, Khatyr F, Garcin C (2008) A new experimental method for measuring skin's natural tension. *Skin Res Technol* 14(1):1–7
- Jeffcoate W, Price P, Harding K (2004) Wound healing and treatments for people with diabetic foot ulcers. *Diabetes Metab Res* 20(Suppl 1):S78–89
- Kessler D, Dethlefsen S, Haase I, Plomann M, Hirche F, Krieg T, Eckes B (2001) Fibroblasts in mechanically stressed collagen lattices assume a synthetic phenotype. *J Biol Chem* 276(39):36,575–36,585
- Kischer C (1975) Alteration of hypertrophic scars induced by mechanical pressure. *Arch Dermatol* 111(1):60
- Lin I, Taber L (1995) A model for stress-induced growth in the developing heart. *J Biomech Eng* 117(3):343
- Maggelakis S (2004) Modelling the role of angiogenesis in epidermal wound healing. *Discrete Contin Syst* 4:267–273
- Martin P (1997) Wound healing: aiming for perfect skin regeneration. *Science* 276(5309):75–81
- Martin P, Lewis J (1992) Actin cables and epidermal movement in embryonic wound healing. *Nature* 360(6400):179–83
- McDougall S, Dallon J, Sherratt J, Maini P (2006) Fibroblast migration and collagen deposition during dermal wound healing: mathematical modelling and clinical implications. *Philos T Roy Soc A* 364(1843):1385–405
- McGrath M, Simon R (1983) Wound geometry and the kinetics of wound contraction. *Plast Reconstr Surg* 72(1):66–72
- Mendez-Eastman S (2001) Guidelines for using negative pressure wound therapy. *Adv Skin Wound Care* 14(6):314–323
- Monaco J, Lawrence W (2003) Acute wound healing an overview. *Clin Plast Surg* 30(1):1–12
- Moulton D, Goriely A (2011) Possible role of differential growth in airway wall remodeling in asthma. *J Appl Physiol* 110(4):1003–12
- North J, Gibson F (1978) Volume compressibility of human abdominal skin. *J Biomech* 11(4):203–207
- Olsen L, Maini P, Sherratt J, Dallon J (1999) Mathematical modelling of anisotropy in fibrous connective tissue. *Math Biosci* 158(2):145–170
- Pierce G, Mustoe T, Lingelbach J, Masakowski V, Griffin G, Senior R, Deuel T (1989) Platelet-derived growth factor and transforming growth factor-beta enhance tissue repair activities by unique mechanisms. *J Cell Biol* 109(1):429–440
- Press W, Vetterling W, Teukolsky S, Flannery B, Greenwell Yanik E (1994) Numerical recipes in fortran-the art of scientific computing. *SIAM Rev* 36(1):149–149
- Rachev A, Stergiopoulos N, Meister J (1998) A model for geometric and mechanical adaptation of arteries to sustained hypertension. *J Biomech Eng* 120(1):9
- Rivlin R (1948a) Large elastic deformations of isotropic materials I. *Philos T Roy Soc A* 240(822):459–490
- Rivlin R (1948b) Large elastic deformations of isotropic materials III. *Philos T Roy Soc A* 240(823):509–525
- Rodriguez E, Hoger A, McCulloch A (1994) Stress-dependent finite growth in soft elastic tissues. *J Biomech* 27(4):455–467
- Segal R, Diegelmann R, Ward K, Reynolds A (2012) A differential equation model of collagen accumulation in a healing wound. *B Math Biol* 74(9):2165–82
- Sherratt J, Murray J (1990) Models of epidermal wound healing. *P Biol Sci* 241(1300):29–36
- Sherratt J, Murray J (1991) Mathematical analysis of a basic model for epidermal wound healing. *J Math Biol* 29:389–404
- Sherratt J, Murray J (1992) Epidermal wound healing: the clinical implications of a simple mathematical model. *Cell Transpl* 1(5):365–371
- Singer A, Clark R (1999) Cutaneous wound healing. *N Eng J Med* 341:738–746
- Taber L (1998) A model for aortic growth based on fluid shear and fiber stresses. *J Biomech Eng* 120(3):348
- Taber L (2001) Biomechanics of cardiovascular development. *Annu Rev Biomed Eng* 3:1–25
- Taber L (2009) Towards a unified theory for morphomechanics. *Philos T R Soc A* 367(1902):3555–83
- Taber L, Eggers D (1996) Theoretical study of stress-modulated growth in the aorta. *J Theor Biol* 180(4):343–57
- Tracqui P, Woodward D, Cruywagen G, Cook J, Murray J (1995) A mechanical model for fibroblast-driven wound healing. *J Biol Syst* 3(4):1075–1084
- Tranquillo R, Murray J (1992) Continuum model of fibroblast-driven wound contraction: Inflammation-mediation. *J Theor Biol* 158(2):135–172
- Uhal B, Ramos C, Joshi I, Bifero A, Pardo A, Selman M (1998) Cell size, cell cycle, and alpha -smooth muscle actin expression by primary human lung fibroblasts. *Am J Physiol Lung Cell Mol Physiol* 275(5):998–1005
- Vermolen F, Javierre E (2012) A finite-element model for healing of cutaneous wounds combining contraction, angiogenesis and closure. *J Math Biol* 65(5):967–96
- Wahl S, Wong H, McCartney-Francis N (1989) Role of growth factors in inflammation and repair. *J Cell Biochem* 40(2):193–9
- Wrobel L, Fray T, Molloy J, Adams J, Armitage M, Sparrow J (2002) Contractility of single human dermal myofibroblasts and fibroblasts. *Cell Motil Cytoskelet* 52(2):82–90
- Wu M, Ben Amar M (2015) Growth and remodelling for profound circular wounds in skin. *Biomech Model Mechanobiol* 14(2):357–370
- Wyczalkowski M, Varner V, Taber L (2013) Computational and experimental study of the mechanics of embryonic wound healing. *J Mech Behav Biomed* 28:125–146
- Yang L, Witten T, Pidaparti R (2013) A biomechanical model of wound contraction and scar formation. *J Theor Biol* 332(null):228–248